JOURNAL OF GUIDANCE, CONTROL, AND DYNAMICS
Vol. 16, No. 2, March-April 1993

Flight-Path Estimation in Passive Low-Altitude Flight by Visual Cues

Arthur J. Grunwald* and S. Kohn†
Technion—Israel Institute of Technology, Haifa 32000, Israel

A series of experiments has been conducted, in which subjects had to estimate the flight path while passively being flown in straight or in curved motion over several types of nominally flat, textured terrain. Three computer-generated terrain types have been investigated: 1) a random "pole" field, 2) a flat field consisting of random rectangular patches, and 3) a field of random parallelepipeds. Experimental parameters were the velocity-to-height (V/h) ratio, the viewing distance, and the terrain type. Furthermore, the effect of obscuring parts of the visual field has been investigated. Assumptions have been made about the basic visual-field information by analyzing the pattern of line-of-sight (LOS) rate vectors (streamers) in the visual field. The experimental results support these assumptions and show that, for both a straight as well as for a curved flight path, the estimation accuracy and estimation times improve, to a certain extent, with the V/h ratio. Error scores for the curved flight path are found to be about 3 deg in visual angle higher than for the straight flight path, and the sensitivity to the V/h ratio is found to be considerably larger. For the straight motion, the flight path could be estimated successfully from local areas in the far field, although at the expense of larger estimation times. However, curved flight-path estimates have to rely on the entire LOS rate pattern rather than on local field estimates.

Introduction

GIBSON[1-3] has shown first that the direction of self-motion can be derived from the motion pattern of texture points in the visual field. He showed that for an observer in rectilinear motion the "optical flowfield" or "streamer" pattern seems to expand from a focal point that indicates the direction of motion. However, in these early studies, no mechanism was suggested for other than straight motion. For curved motion, for instance, the converging pattern of streamers tends to "bend" sidewards, and the "focus of expansion" is no longer defined. Gordon[4,5] has given an analytical description of the flowfield for curved motion in car driving, but did not mathematically model how the driver derives control-oriented visual-field information from this flowfield. Warren[6,7] has summarized and improved Gibson's work and has performed detailed experimental studies of self-motion estimation in straight and level flight. Since then, several analytical and experimental studies have investigated the problem of deriving self-motion parameters of arbitrary motion, from the optical flowfield pattern while flying over arbitrary, nonflat terrain: Zacharias et al.[8,9] This is known as the "inverse" flowfield solution. A significant contribution of their work is that in addition to the self-motion parameters, the inverse solution is able to compose an "impact time" map of the terrain structure as well. Other visual-field studies investigate the visual cues used in self-motion forward speed perception and control: Denton,[10] Owen et al.,[11] Awe et al.,[13] and Larish and Flach.[14] They conclude that "edge rates" (the frequency of passing texture units) rather than "flow rates" are used as the main cue for speed control. Johnson et al.[12] studied vertical hovering control and conclude that in the presence of forward/lateral disturbing motion, forward looking optical density and vertical optical motion, rather than changes in optical splay, are the primary cues for altitude control.

Although the previously mentioned studies were focused on identifying the essential visual cues during motion, other studies have evaluated visual-field information models in pilot-in-the-loop simulations. Naish[15] has used the familiar shape and size of the runway for determining aircraft positional, attitude, and flight-path information. Wewerinke[16,17] has used a similar visual model in an optimal control framework for studying the pilot response. Similar optimal control frameworks have been used by Grunwald and Merhav[18-20] for incorporating a visual cueing model based on the visual-field "streamer pattern," and lately by Schmidt and Silk[21] to study the estimation accuracy of the aircraft response based on visual cues derived from the horizon and the runway image. Common to all of these studies is the notion that the visual-field information is derived from different areas of the visual field, and the sophisticated analytical and experimental efforts to identify these areas.

This research has been motivated by the need for understanding the control-oriented visual-field information in helmet mounted display (HMD) nap-of-the-earth (NOE) helicopter flight. The image of a Forward Looking Infrared Radiation (FLIR) camera, gimbal mounted at the front of the helicopter, is transferred to a miniature helmet mounted CRT. By means of collimating optics and a beam splitter, the image is shown to a single eye and appears to be superimposed on the visual field at infinity. The camera is slaved to the pilot's head motions, so that, in spite of the relatively narrow visual field of the helmet mounted display, a large area of the outside scene can be covered.

This paper summarizes baseline experiments of a more comprehensive program, aimed at understanding the visual-field information in helmet mounted displays. The purpose of these experiments is to obtain baseline measurements of a subject's ability to derive the visual-field information from a wide-angle visual field. Therefore, in this experiment, the visual field is presented on a wide-angle display monitor. In ongoing research, the experiment is being repeated for an identical visual situation, viewed through a HMD. Both the baseline wide-angle experiment and the HMD experiments deal with a stationary visual field, i.e., the observer is either in straight or steady curved motion. Although in actual NOE flight the flight path might be arbitrary, it can be considered to consist of a set of piecewise constant straight or constantly curved sections.

Received Sept. 10, 1990; revision received May 28, 1992; accepted for publication June 4, 1992.

*Senior Lecturer, Faculty of Aerospace Engineering. Member AIAA.

†M.Sc Graduate Student, Faculty of Aerospace Engineering.

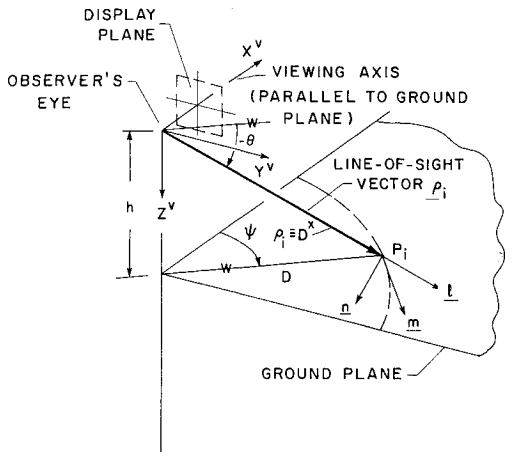

Fig. 1 General viewing situation.

Visual Flowfield Cues in Straight and Curved Flight

Straight Flight

The general viewing situation is shown in Fig. 1. The observer's viewing system is $x^v y^v z^v$, with the observer's eye at its origin. The x^v axis is the viewing axis, parallel to the ground plane and perpendicular to the display plane; the y^v axis is parallel to the ground plane and points to the right; and the z^v axis points downwards. The height of the observer's eye above the ground plane is h. Consider a conspicuous point on the ground plane, P_i. The line-of-sight (LOS) vector to P_i is ρ_i, and the viewing azimuth and elevation angles of P_i are ψ and θ, respectively (θ is negative for ρ_i pointing downward). The viewing range measured along the ground plane is D and the range measured along the LOS is $D^* \equiv \rho_i = (D^2 + h^2)^{1/2}$.

The horizontal situation of rectilinear level flight over flat terrain is shown in Fig. 2a. The angle between the viewing axis x^v and the velocity vector $\bar{V}$ is the crabbing angle β. For natural visual flight, using the through-the-windshield visual field, the viewing axis aligns with the longitudinal vehicle axis and β will be the vehicle sideslip angle. For visual flight by teleoperated helmet mounted displays, the viewing axis aligns with the camera axis, which can be rotated with respect to the vehicle axis by any arbitrary head angle. In that case β will be the vehicle sideslip angle minus the head angle.

Consider a set of conspicuous points, $P_1, P_2, \ldots, P_n$, on the terrain surface at viewing range D, equally spaced in azimuth angle. The trajectories, traced by each one of these points in the moving reference frame of the observer, are straight lines, parallel to $\bar{V}$. Figure 2b shows these lines, mapped on a unity sphere, centered about the observer's eye (the viewing sphere). The horizontal and vertical axes in Fig. 2b are the viewing azimuth angle ψ and the viewing elevation angle θ, respectively.

Resulting from the observer's self-motion, the LOS vector ρ_i will change with time. The time derivative $\dot{\rho}_i$ is given by

$$\dot{\rho}_i = -\omega \times \rho_i - V \tag{1}$$

where ω and V are the rotational and translational self-motion vectors, respectively. It is useful to decompose $\dot{\rho}_i$ in a LOS centered system, l, m, and n; see Fig. 1. The l axis points along the LOS vector, the m axis is perpendicular to it and is also parallel to the ground plane, and the n axis is orthogonal to l and m, and points downward for a right-hand system. The m and n components of $\dot{\rho}_i$, divided by its length $D^* \equiv \rho_i$, are the sensed horizontal (azimuth) and vertical (elevation) components of the apparent LOS motion. The ratio ν between the horizontal and the vertical components defines the apparent LOS direction of motion. Expressions for these components, as a function of viewing azimuth and viewing range D, are derived in the Appendix.

Although trivial, it is vital to recognize that in the observer's system each point will have an apparent LOS motion, which aligns with the trajectories of Fig. 2b. The visual flowfield can be defined as the pattern of apparent LOS motion of conspicuous surface points ("streamers"). For rectilinear flight, this pattern appears to expand from a common focal point on the horizon, point F; see Fig. 2b. The straight vehicle path is defined by the set of points that do not have an azimuth velocity component, i.e., points for which the m component of the LOS rate vector is zero; see the solid vertical line in Fig. 2b. This is the case for points with viewing azimuth β. For these points the ratio ν is zero, and the LOS direction of motion is apparently vertical, i.e., perpendicular to the horizon or to the y^v axis for zero vehicle roll angle. The detectability of the azimuth for which $\nu = 0$ depends on the derivative of ν with respect to the azimuth angle ψ. This quantity, $\lambda = \partial\nu/\partial\psi$, is hereafter referred to as the "local expansion" of the field. The larger the local expansion, the easier it will be to pick the apparent vertical LOS motion from a "bundle" of streamers. It is shown in the Appendix that for straight flight $\lambda = -D^*/h$. Thus, λ is independent of the azimuth and proportional to D^*.

It is shown in the Appendix that LOS rate magnitudes for points on the vehicle path are inverse proportional to $(D^*)^2$. Detectability of the apparent vertical streamer both depends on the LOS rate magnitude and on the local expansion. The LOS rates are the largest in the "near" visual field and the local expansion the largest in the "far" field. However, in the very near field the angular rates might be too large and induce blurring of the image and in the very far field the angular rates might be below the threshold of detection. Any viewing range in between will enable the estimation of the local area streamer

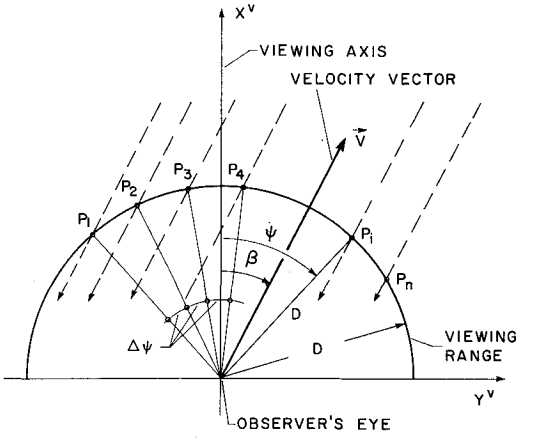

Fig. 2a Horizontal situation for rectilinear level flight.

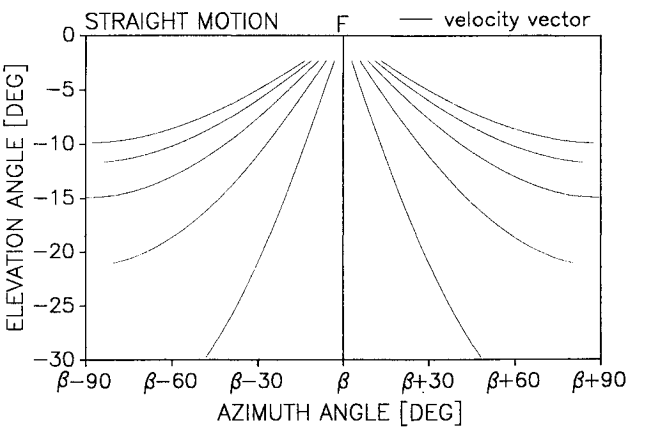

Fig. 2b Pattern of apparent line-of-sight motion (streamers) for rectilinear level flight.

direction. A possible mechanism for estimating the straight vehicle path is to select the apparent vertical streamer from a local area in the visual field, at the farthest viewing distance at which the streamer direction can still be detected, and at which the local expansion λ is the largest. The estimation of the complete path can be achieved simply by extrapolating a vertical line through the selected vertical streamer in this local area.

Curved Flight

The mechanism for estimating the flight path in steady curved flight is far more complex. The horizontal situation of steady curved flight over flat terrain is shown in Fig. 3a. The instantaneous velocity vector is $\bar{V}$, and β is again the crabbing angle. However, the actual vehicle path is a circle with radius R_o, tangential to V and with its center at point M. Again, consider a set of points at given viewing range D, equally spaced in azimuth angle. The trajectories, traced by each one of these points, are concentric circles with M at their center. Figure 3b shows these trajectories mapped on the viewing sphere. The pattern of velocity vectors shows a converging, curved set of lines, and a common focal point on the horizon no longer exists. The curved vehicle path is the dashed, central line in the bundle. The vehicle path is defined by the trajectory traced by points, which, for very close viewing ranges, will

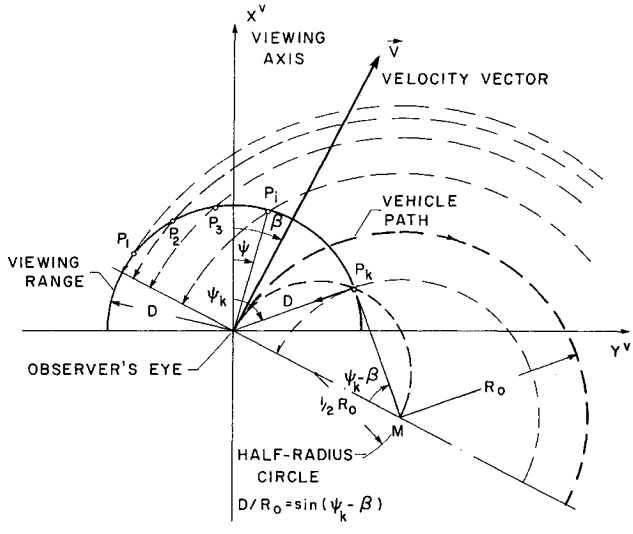

Fig. 3a Horizontal situation for curved level flight.

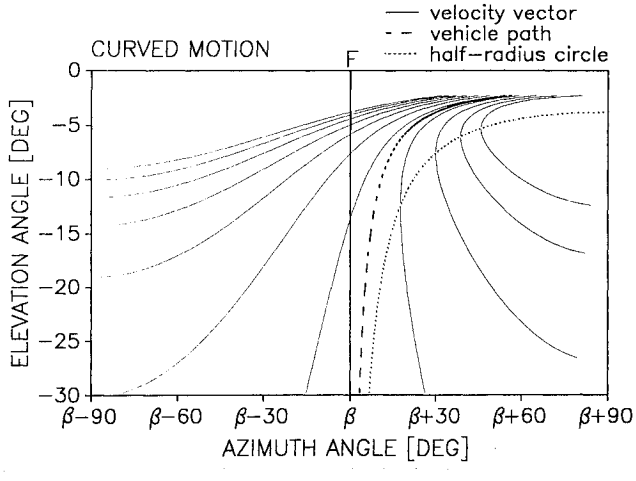

Fig. 3b Pattern of apparent line-of-sight motion (streamers) for curved level flight.

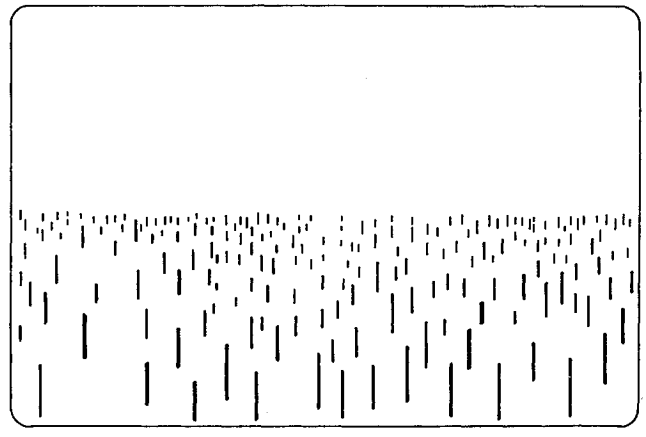

Fig. 4a Perspective view of the field of randomly placed poles.

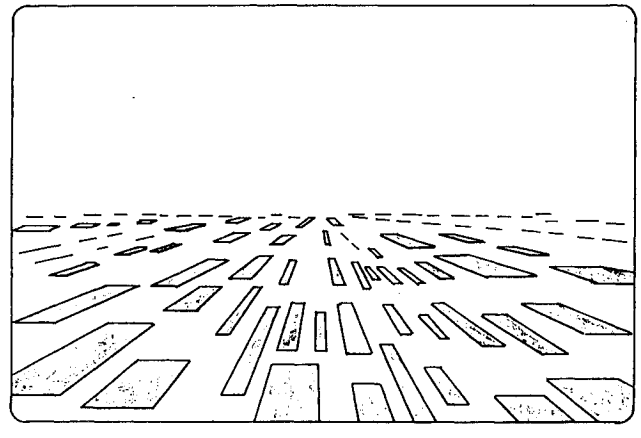

Fig. 4b Perspective view of the field of rectangular patches.

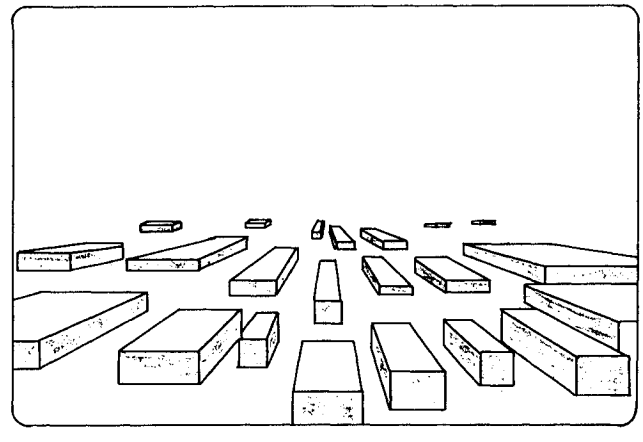

Fig. 4c Perspective view of the field of parallelepipeds.

have a zero azimuth LOS motion component and which tend to move tangential to the velocity vector (solid vertical line).

It is interesting to consider other points in the visual field, which do not have an azimuth LOS motion component. It is clear from Fig. 3a that the locus of these points is formed by the circle, tangential to $\bar{V}$ and with radius $0.5R_o$, hereafter referred to to as the "half-radius circle." This locus is shown in Fig. 3b as the dotted line. For $D \ll R_o$, the azimuth angle of a point on the vehicle path is about halfway in between the azimuth angle of the velocity vector and of a point on the half-radius circle.

Several mechanisms for detecting the curved vehicle path can be thought of. All of these mechanisms would process the

pattern of apparent LOS motion in the visual field. A first possible mechanism for estimating a point on the vehicle path is to look for the azimuth angle of the area at viewing distance D, with a zero azimuth LOS motion component (on the half-radius circle). Next, the azimuth of the velocity vector would be estimated by looking, at very close distances, for points with a zero azimuth LOS motion component. It would then estimate the azimuth of a point on the vehicle path at distance D to be halfway in between the two angles. A shortcoming of this mechanism is that it will break down when the point on the half-radius circle is outside the field of view.

A second mechanism would look for continuity of motion between points in the visual field. It would select a set of points that belong to a certain section of the streamer, by following the motion of a texture point over a given interval of time. Next, the correspondence would be found between streamer sections that would add up to the central streamer, i.e., the one of which the azimuth LOS motion component for close viewing distances is zero, or, alternatively, the streamer, which tends to be tangential to the apparent vertical.

A third mechanism of a less-descriptive nature would process a set of flowfield measurements, i.e., pairs of LOS vectors and their angular rates, to compute the observer's translational and rotational self-motion. This method is well known in computer vision, and has been successfully used as a model for human visual flowfield cueing by Zacharias et al.[8,9] An interesting finding of their work is that a flowfield measurement has to satisfy certain conditions in order to be effective in the self-motion estimation process, and that therefore not all areas of the visual field are useful.

Common to all of these mechanisms is the need for processing information in the far as well as in the near visual field. This is in contrast to the estimation of the straight path, where it would be sufficient to consider one local area in the far field only.

A case of curved flight of special interest is the one in which the crabbing angle β is zero. In this case, the velocity vector is at a viewing azimuth of zero, at the center of the visual field, and thus does not have to be derived from the visual field. This occurs in through-the-windshield coordinated visual flight in the absence of steady side winds, but also in car driving. Here the requirements on processing the near visual field are less demanding. On the other hand, in helicopter flight by teleoperated helmet mounted displays, both nonzero vehicle sideslip angles and considerably large head angles might occur. In this case, the velocity vector might be considerably off-centered at an unknown azimuth. In the absence of specific symbology, head rotation becomes indistinguishable from vehicle yaw rotation. In this case, the estimation of the vehicle path will have to rely strongly on the near visual field.

Experimental Program

Purpose of the Experiment

The purpose of the experiment was to investigate the ability of an observer to estimate the flight path in straight and curved level passive flight, from the visual field, as a function of the velocity-to-height ratio, the terrain type, the viewing distance, and under conditions of a partially obscured visual field. In view of teleoperated helmet mounted displays, it is of particular interest to investigate whether and to which extent curved flight-path estimates are affected by constant and unknown sideslip angles.

Experimental Setup

The visual scene was generated at a Silicon Graphics IRIS 4D 50/GT workstation. The image measured 13.5 in. horizontally and 10.8 in. vertically, and the subject was viewing the image monoscopically through a fixed aperture from a distance of 5.4 in. The eye was placed at the station point of the image. Thus, the field of view was 102.7 deg horizontally and 90 deg vertically. Each trial represented either rectilinear or curved level flight over nominally flat terrain. The viewing axis was parallel to the ground plane and was represented by the center of the display. The direction of motion $\overline{V}$ was deviating from the viewing axis by the sideslip angle β, and the curved path was tangential to $\overline{V}$. The terrain was visible from a distance of 1.0 units of the height h of the observer above the ground (bottom edge of the screen) until $15h$ (far end of the field).

The subject initiated an experimental trial by pressing a mouse button, after which the visual field became visible from an initially blank screen. For each trial, the sideslip angle β and/or the path curvature radius R_o were uncorrelated and each one chosen from a uniformly distributed random set of values. A response marker was visible in the visual field at viewing distance D, consisting of a circular base of diameter $0.625h$ placed in the ground plane and a vertical pole at its center of height $0.125h$. By moving the mouse left/right, the subject could change the azimuth angle of the marker, while D remained constant (the marker thus moved along part of a circle with the observer at the center). The subject was asked to place the marker on the estimated flight path. He was instructed to do this intuitively, as quickly as possible, and to acknowledge his choice by pressing a mouse button. During the training runs, after each trial, a dotted line with a second marker half of the size of the first one was displayed, indicating the true flight path and the location on this path at viewing range D. This marker remained visible for 2 s.

Experimental Program

Three types of experiments were conducted: 1) straight and level flight in the presence of a constant, randomly chosen sideslip angle; 2) steady, randomly chosen curved and level flight with zero sideslip; and 3) steady curved and level flight with constant, randomly chosen sideslip.

The relevant parameters investigated were the velocity-to-height ratio, the viewing distance at which the response marker was placed, and the type of terrain. Five velocity-to-height ratios were chosen, ranging from 0.25 to 4 s^{-1}. Two response marker viewing distances were chosen: $D = 7.5h$ for the far field and $D = 1.5h$ for the near field. The three terrain types are shown in Figs. 4a–c and were 1) a field of randomly placed poles with constant density and with no visible alignment; 2) a field of rectangular patches that were of random shape and size and randomly placed in a cross-grid pattern, and which showed distinct alignment, like a cultivated agricultural field; and 3) like the field of rectangles, but consisting of parallelepipeds, simulating buildings. The average distance between the poles in the x^v and y^v directions was $0.83h$ each, and their average height was $0.25h$. The average length and width of the rectangles was $0.385h$, and the average distance between their centers in the x^v and y^v directions was $0.625h$. For the buildings the average length and width was $0.277h$, the average height $0.285h$, and the average distance between their centers in the x^v and y^v directions was $1.25h$.

In addition to the above-mentioned parameters, the effect of obscuring parts of the visual field was investigated. Two cases were considered: for the response marker at the far viewing distance, $D = 7.5h$, the near visual field was obscured, so that the terrain was only visible from $5h$ until $15h$; and for the near response marker viewing distance, $D = 1.5h$, the far visual field was obscured and the terrain was visible from $1.0h$ until $5h$.

In the straight-motion experiment, the constant sideslip angle β was chosen from a uniformly distributed random set, ranging from -45 to $+45$ deg. In the curved-motion experiment, both β and the path curvature radius R_o were chosen from uncorrelated, uniformly distributed random sets. The range for β was from -14 to $+14$ deg and the range for the path curvature radius R_o from $15h$ to $40h$, where the curvature could be to the left or to the right at random with equal probability.

Subject Background, Training, and Experimental Procedure

The subjects consisted of eight males and one female, all of which were Technion Aerospace undergraduate students. Subject age was between 19 and 24. After two 1-h training sessions, each subject carried out a series of runs for each one of the three experiments (straight, curved, curved with sideslip, in this order). Each series included 16 configurations (V/h ratio, viewing distance D, terrain type, obscuration type) each of which was repeated four times and addressed in a random fashion. Each configuration consisted of a set of 20 consecutive trials, each of which was initiated by the subject by pressing a mouse button. Each trial lasted for about 2–8 s, depending on the time needed by the subject to estimate the direction of motion. Eight 1-h sessions were needed for each subject to finish the experimental program.

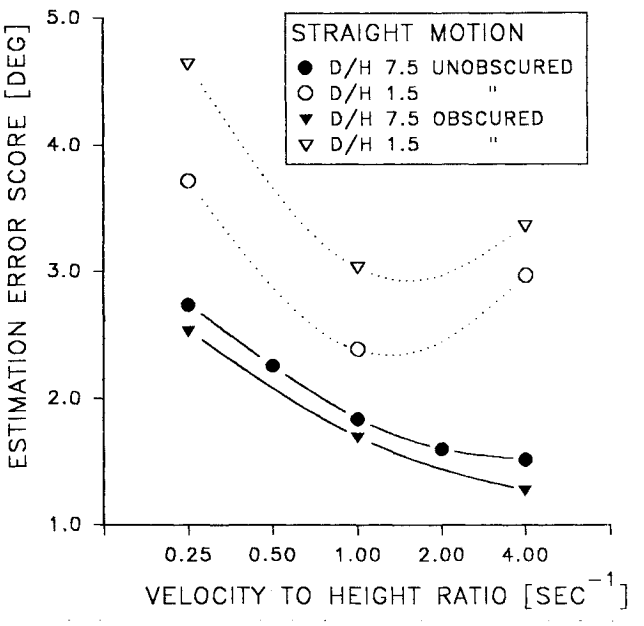

Fig. 5a Averaged estimation error score vs the V/h ratio, for straight flight for the "pole" field, for $D = 7.5h$ and $D = 1.5h$ (unobscured and obscured cases).

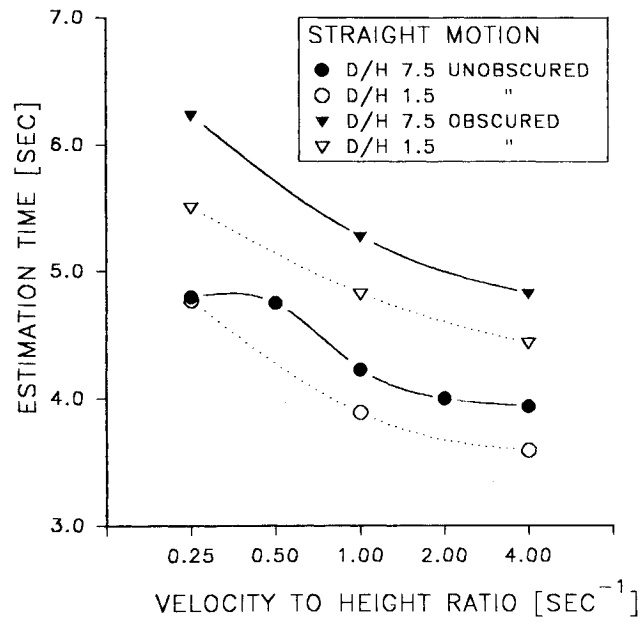

Fig. 5b Averaged estimation time vs the V/h ratio, for straight flight for the "pole" field, for $D = 7.5h$ and $D = 1.5h$ (unobscured and obscured cases).

Subject motivation was enhanced by a reward system based on competition. After each set of 20 trials, the subject's overall performance score was displayed, based on a weighted average between estimation error and estimation time. Subjects were divided in four groups. The subject with the best score in each group was given double pay, and the one with the best score of all groups was given triple pay.

Experimental Measurements

For each trial in a set, the error in azimuth angle between the true and estimated location of a point on the flight path at response marker viewing distance D was recorded, together with the time needed to make the estimate. The upper limit on the estimation time was 8 s, after which the run was terminated and marked as a failed run.

Experimental Results

Processing of Measurements

For each set of 20 trials, the average and the standard deviation of the estimation error and estimation time were computed. For all three experiments, the average of the estimation error was found to be nominally zero, i.e., no preference for an error in left or in right direction was found. The standard deviation of the estimation error generally reflects the accuracy at which a point on the flight path can be estimated, and this value was taken as the estimation error score of each set. For the estimation time, the average of the set was taken as the representative score.

Results for Straight Motion

Effect of the Velocity-to-Height Ratio

Figure 5a shows the averaged estimation error score as a function of V/h for the pole field and for the response marker at the "far" viewing distance $D = 7.5h$. The error score decreases monotonically with increasing V/h, from 2.74 deg at $V/h = 0.25$ s^{-1} to 1.52 deg at $V/h = 4$ s^{-1}. This means that by increasing the velocity by a factor of 8, the estimation accuracy increases by 45%. This supports the results of a similar experiment by Warren[6] in which error scores of 1.5 deg were reported.

Figure 5b shows the effect of V/D on the averaged estimation time. The estimation time also decreases with increasing V/h from 4.8 s at $V/h = 0.25$ s^{-1} to 3.94 s at $V/h = 4$ s^{-1}. Thus, for the "far" viewing distance, higher velocities enable both faster and more accurate estimates. This was expected, since larger V/h ratios yield larger LOS rates, which result in larger apparent displacements of texture points in a given time frame. This allows the apparent LOS direction of motion to be estimated more accurately or, equivalently, allows shorter estimation times for obtaining a given accuracy.

Effect of the Viewing Distance for Unobscured Visual Field

Figure 5a shows the effect of the viewing distance on the V/h dependency. The curve for the "near" viewing distance $D = 1.5h$ for the same pole field is markedly above the one for the far viewing distance. This indicates that estimating the direction of motion from the near field is much less accurate. Although the LOS rates are larger in the near field, finding the apparent vertical streamer is harder because of the substantially smaller local expansion λ. It is also seen that in particular for the high velocity, $V/h = 4$ s^{-1}, the accuracy is markedly less. This might result from blurring due to the very fast motion in the near field.

Figure 5b shows that the curve for the average estimation time, for the near viewing distance, is somewhat below the one for the far viewing distance. This again supports the assumption that in the presence of larger LOS rates, it takes less time to estimate the apparent LOS direction of motion. Furthermore, for the very fast velocities, it is generally more difficult to view the fast motion in the near field for a prolonged time.

Effect of the Terrain Type

The effect of the terrain type is shown in the bar graphs of Figs. 6a and 6b. The pole field yields the best accuracy and estimation time, and the field of rectangles the worst (error scores 18% and estimation times 6% above average). The accuracy and estimation time for the parallelepipeds is only slightly worse than that of the pole field. The pole field differs from the field of rectangles and parallelepipeds in the sense that no distinct cross-grid direction exists. The field of rectangles differs from the other two in the sense that the third dimension of the height is missing. The results in Figs. 6a and 6b show that the height dimension contributes to a faster and more accurate estimate. On the other hand, the effect of the existence of a cross grid is much smaller. A possible explanation for this is that, in the presence of the height dimension, the subjects might have used some motion parallax scheme in order to detect azimuth LOS rates. A different explanation is that the height dimension might have contributed to a better awareness of the apparent local vertical, which, in turn, allowed the apparent vertical LOS motion to be detected more accurately.

Effect of Partial Obscuring of the Visual Field

The effect of partial obscuring of the visual field is shown in Figs. 5a and 5b, which show that for the "close" viewing distance obscuring of the far field shifts the curve upward by an average of 0.7 deg. This is in contrast with the curve for the "far" viewing distance, where obscuring of the close field shifts the curve downward by an average of 0.2 deg. This clearly indicates that, for the unconstrained viewing situation, vital information is derived from the far field, in spite of the fact that the response marker appears in the near field. On the other hand, obscuring the near field does not affect the accuracy negatively. Therefore, the far field in this rectilinear direction estimation task is essential.

However, the effect of obscuring the near field is strongly noticed in the curves for the estimation time; see Fig. 5b. The curve shifts upwards by an average of 1.13 s. This indicates that although the accuracy is not affected by obscuring the near field, markedly longer estimation times are needed. A similar effect is noticed for the curves for the near viewing distance. Obscuring the far field shifts the curve upward by an average of 0.84 s. This supports the assumption that the far field with its substantially larger local expansion allows the apparent vertical LOS motion to be detected more accurately, but, as a result of the lower LOS rates, requires more time.

Results for Curved Motion

Effect of the Velocity-to-Height Ratio

The solid curves in Fig. 7a show the averaged estimation error score as a function of V/h for the pole field and the response marker at the "far" viewing distance $D = 7.5h$. The error score for curved flight decreases strongly with increased V/h ratio, with a minimum at $V/h = 2\ s^{-1}$, and is on the average about 3 deg higher than for straight flight. The downslope of the V/h dependency for curved flight is markedly larger than for straight flight. This indicates that for curved flight the estimation accuracy is more sensitive to the LOS rate magnitude. This was expected, since curved flight-path estimation relies on a larger portion of the flowfield pattern, rather than finding a specific area with apparent vertical LOS motion. Obviously, the ability to perceive this pattern improves with LOS rate magnitude. Figure 7a also shows that for $V/h = 4\ s^{-1}$ the error score is about 1 deg above the one for $V/h = 2\ s^{-1}$. An explanation for this is that the near-field motion is so fast that blurring occurs, resulting in higher error scores.

Figure 7b shows the curves for the estimation time. Generally, the estimation time reduces with increased V/h ratio. This confirms the findings for the straight motion that, due to a higher LOS rate magnitude, it will take less time to estimate the apparent LOS direction of motion with a given accuracy.

Effect of the Viewing Distance

The dotted curves in Fig. 7a show the V/h dependency for the close viewing distance $D = 1.5h$. The error score curve for the same pole field is initially almost level with its minimum at $V/h = 1\ s^{-1}$. For values of V/h larger than $1\ s^{-1}$, the error score increases strongly. This indicates that in the near field, for the low V/h ratios, the LOS rate magnitude is already at such a level that an additional increase does not contribute to a better estimate. Beyond $V/h = 1\ s^{-1}$ the error scores increase strongly, probably as a result of the effect of image blurring.

Comparison of the V/h dependencies for far and close viewing distances shows that for $V/h = 0.25\ s^{-1}$ the close viewing distance is superior, and for $V/h = 4\ s^{-1}$ the far viewing distance is superior. The "crossover" is at about $V/h = s^{-1}$.

The curves for the estimation time in Fig. 7b show also for the close viewing distance $D = 1.5h$ a general reduction in estimation time with increased V/h ratio. The estimation times for curved flight are on the average slightly larger than for straight flight. Figure 7b also shows that the estimation

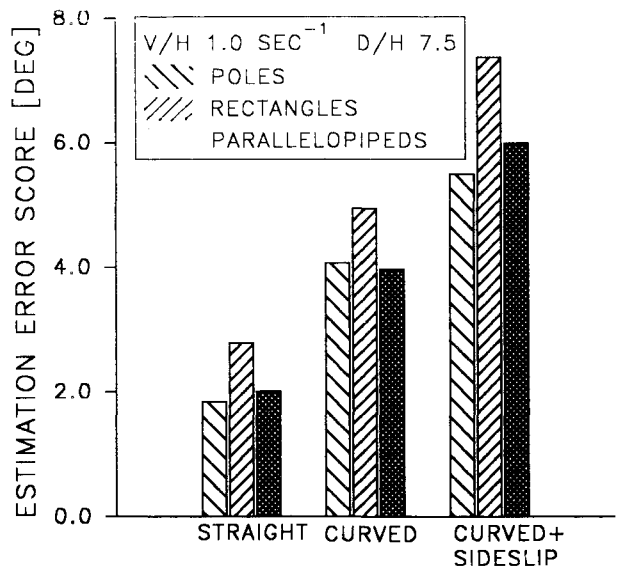

Fig. 6a Effect of the terrain type on the averaged estimation error score (for $V/h = 1.0\ s^{-1}$ and $D = 7.5h$).

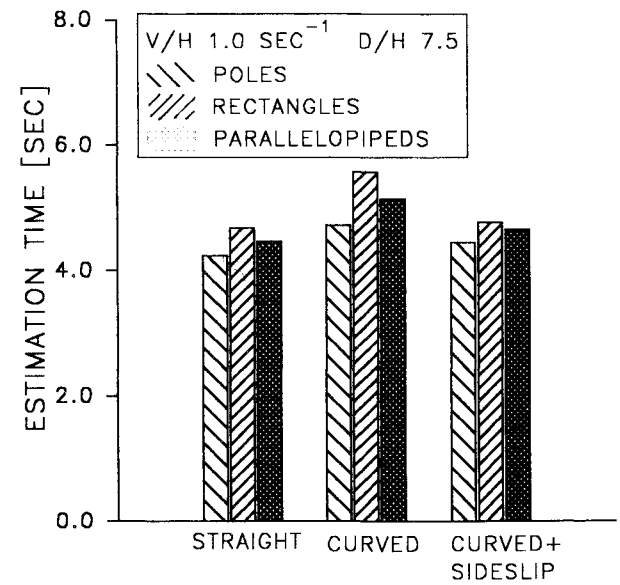

Fig. 6b Effect of the terrain type on the averaged estimation time (for $V/h = 1.0\ s^{-1}$ and $D = 7.5h$).

time curve for the close viewing distance is on the average about 0.6 s below the one for the far distances. This again supports the notion that for the near field the subjects act faster because it is more difficult to view the fast motion for a prolonged time.

Effect of Sideslip

The effect of sideslip for the far viewing distances is shown in Fig. 7a. The error score curves for motion with and without sideslip have very similar characteristics, i.e., a similar downslope and minimum at $V/h = 2\ s^{-1}$. However, the curve for motion with sideslip is on the average about 1.2 deg above the one for motion without sideslip. This was expected, since in the first case, in the process of estimating the vehicle path, the observer has to derive the direction of motion from the near visual field, whereas in the latter case the direction of motion is presented to him implicitly by the center of the display. It should be noted that the increase in error of 1.2 deg relates to an average stimulus sideslip angle of 7.5 deg. This proves that the observer is able, to a large extent, to estimate the constant, unknown, randomly chosen, direction of motion. Figure 7a further shows that the difference between the curves with and without sideslip increases with the V/h ratio. Since the additional information required in the case of motion with sideslip originates from the near visual field, and since this information deteriorates with the V/h ratio, this increased error score was expected (see also straight flight, obscured far field; Fig. 5a).

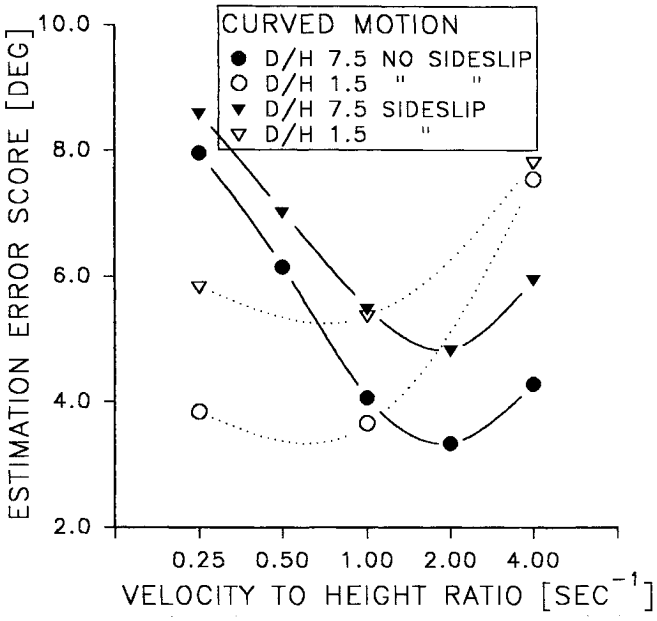

Fig. 7a Averaged estimation error score vs the V/h ratio (curved motion with and without sideslip; comparison between close and far viewing distances).

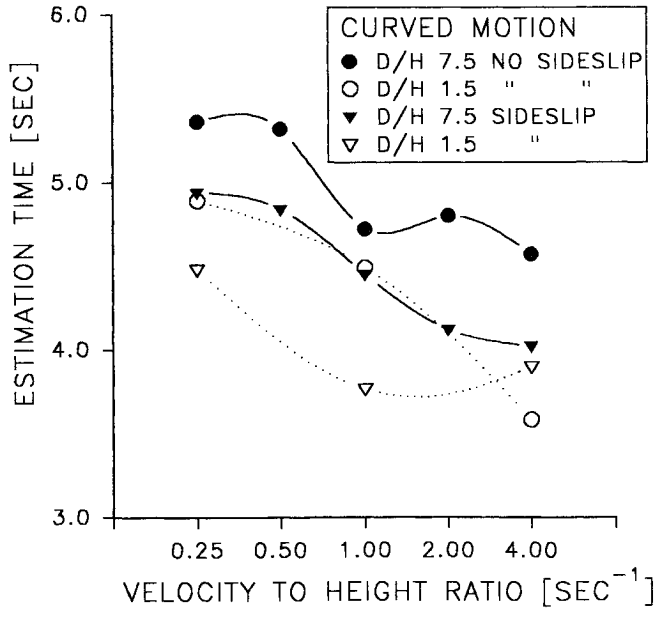

Fig. 7b Averaged estimation time vs the V/h ratio (curved motion with and without sideslip; comparison between close and far viewing distances).

Figure 7b shows the effect of sideslip on the estimation time, for the far viewing distances. The curve for motion with sideslip is similar to the one for motion without sideslip, but is on the average about 0.5 s lower. A similar effect is found for the close viewing distances. It can be speculated that for motion with sideslip the observer's attention is allocated to a larger extent in the close field, which might result in reduced estimation times.

Effect of the Terrain Type

The effect of the terrain type on the error scores for the two types of curved motion is shown in the bar graphs of Figs. 6a and 6b, and closely resemble the straight-motion case. The field of rectangles is in all three cases the worst, and the pole field and field of parallelepipeds yield similar performances. The estimation time for curved motion with sideslip is less consistent with the other configurations. Here the pole field has the longest estimation times.

Concluding Remarks

For an observer in rectilinear level motion, the accuracy in estimating the direction of motion, monotonically increases with the V/h ratio. The time needed to make the estimate decreases monotonically with the V/h ratio. Because of the larger "local expansion," far viewing distances yield more accurate estimates than close viewing distances. However, due to lower LOS rates, the estimates for far viewing distances, take longer. The "height" dimension of the field structure contributes to faster and more accurate estimates. The existence of a distinct cross-grid direction in the field has little or no effect on the accuracy and estimation time. For straight flight and for far viewing distances, obscuring the "near" visual field does not affect estimation accuracy, but yields markedly larger estimation times. For close viewing distances, obscuring of the "far" visual field results in both lower accuracy and larger estimation times. Therefore, for straight flight, the far field is essential in estimating the flight path. The flight path for curved motion is considerably more difficult to estimate than for straight motion, since it relies on the entire LOS rate pattern rather than on local field estimates. Curved flight-path estimates are therefore more sensitive to the V/h ratio. The presence of a constant, randomly chosen, unknown sideslip angle increases the curved flight-path estimation error scores by about 1 deg and demands active use of the near field.

Appendix

Figure 1 shows the spatial situation of the line-of-sight (LOS) to the ith point P_i. The LOS vector is $\boldsymbol{\rho}_i \equiv \text{col}[x, y, z]_i = \text{col}[D\cos\psi, D\sin\psi, h]_i$ and its time derivative is $\dot{\boldsymbol{\rho}}_i \equiv \text{col}[v_x, v_y, v_z]_i$, where col denotes a column vector, D is the viewing range measured along the surface, ψ is the viewing azimuth angle, and h the height above the surface. The $\boldsymbol{m}$ and

$\boldsymbol{n}$ unity vectors of the LOS centered system for azimuth and elevation, respectively, are given by

$$\boldsymbol{m} = \frac{1}{D}\begin{bmatrix} -y \\ x \\ 0 \end{bmatrix}; \qquad \boldsymbol{n} = \frac{1}{DD^*}\begin{bmatrix} -xz \\ -yz \\ D^2 \end{bmatrix} \tag{A1}$$

$$D^* \equiv \rho_i = (D^2 + h^2)^{1/2}$$

where D^* is the viewing range measured along the LOS. The components of $\dot{\boldsymbol{\rho}}_i$ in $\boldsymbol{m}$ and $\boldsymbol{n}$ direction are given by

$$\dot{\rho}_i^m = \boldsymbol{m} \cdot \dot{\boldsymbol{\rho}}_i = 1/D\,(-yv_x + xv_y) \tag{A2a}$$

$$\dot{\rho}_i^n = \boldsymbol{n} \cdot \dot{\boldsymbol{\rho}}_i = -z/DD^*(xv_x + yv_y) \tag{A2b}$$

where $(\cdot)$ denotes the inner product. For circular flight with sideslip β, the translational self-motion vector is given by $\boldsymbol{V} = \text{col}[V\cos\beta, V\sin\beta, 0]$ and the rotational vector by $\boldsymbol{\omega} = \text{col}[0, 0, V/R_o]$, where R_o is the turn radius. The LOS vector rate is then given by

$$\dot{\boldsymbol{\rho}}_i = -\boldsymbol{\omega} \times \boldsymbol{\rho}_i - \boldsymbol{V} = V\begin{bmatrix} y/R_o - \cos\beta \\ -x/R_o - \sin\beta \\ 0 \end{bmatrix} \tag{A3}$$

Substituting Eq. (A3) into Eqs. (A2a) and dividing by the LOS vector length D^* yields the sensed azimuth and elevation (downward positive) LOS rotation, s_{azim}, and s_{elev}, respectively:

$$s_{\text{azim}} = V/D^*[-D/R_o + \sin(\psi - \beta)] \tag{A4a}$$

$$s_{\text{elev}} = hV/(D^*)^2[\cos(\psi - \beta)] \tag{A4b}$$

It is clear from Eq. (A4a) that for $\psi = \beta$ (looking in the direction of motion) and that for $h \ll D$, or $D \cong D^*$, $s_{\text{azim}} \cong V/R_o$, so that the lateral LOS rotation is independent from the viewing distance. Furthermore, Eq. (A4b) shows that the vertical LOS rotation is independent from R_o. The total LOS rotation is given by

$$s_{\text{tot}} = (s_{\text{azim}}^2 + s_{\text{elev}}^2)^{1/2} \tag{A5}$$

For rectilinear flight, and for points on the vehicle path, i.e., points for which $\psi = \beta$, it follows from Eq. (A4a) that $s_{\text{azim}} = 0$. Thus, for given D, $s_{\text{tot}} = s_{\text{elev}}$ is at a minimum, and inverse proportional to $(D^*)^2$. For curved flight the loci of points for which at given D, s_{tot} is minimal, is found by substituting Eqs. (A4) into Eq. (A5), and setting the derivative of s_{tot} with respect to ψ to zero. The loci of minima satisfy the expression:

$$\sin(\psi - \beta) = (D^*)^2/DR_o \cong D/R_o \tag{A6}$$

It is clear that for $h \ll D$, or $D \cong D^*$, the loca of minima coincide with the half-radius circle; see Fig. 3a.

The derivative of the apparent LOS direction $\nu = s_{\text{azim}}/s_{\text{elev}}$ with respect to ψ is defined as the "local expansion," and is given by

$$\lambda \equiv \frac{\partial \nu}{\partial \psi} = \frac{-D^*}{h}\left[1 + \frac{D}{R_o}\frac{\sin(\psi - \beta)}{\cos^2(\psi - \beta)}\right] \tag{A7}$$

Equation (A7) shows that for $\psi = \beta$ or for $R_o \to \infty$ the local expansion is independent of ψ and equals $\lambda \equiv -D^*/h = \sin^{-1}\theta$.

Acknowledgments

This research has been supported by a research grant from NASA Ames Research Center, Aerospace Human Factors Division, Moffett Field, CA 94035, under cooperative agreement No. NAGW-1128. S. Hart and D. Foyle of Ames Research Center have been the Scientific Monitors for this grant.

References

[1]Gibson, J. J., *The Perception of the Visual World*, Houghton Mifflin, Boston, MA, 1950.

[2]Gibson, J. J., Olum, P., and Rosenblatt, F., "Parallax and Perspective During Aircraft Landings," *American Journal of Psychology*, Vol. 68, 1955, pp. 372–385.

[3]Gibson, J. J., "Visually Controlled Locomotion and Visual Orientation in Animals," *British Journal of Psychology*, Vol. 49, 1958, pp. 182–194.

[4]Gordon, D. A., "Static and Dynamic Visual Fields in Human Space Perception," *Journal of the Optical Society of America*, Vol. 55, 1965, pp. 1296–1303.

[5]Gordon, D. A., "Perceptual Basis of Vehicular Guidance," *Public Roads*, Vol. 34, 1966, pp. 53–68.

[6]Warren, R., "The Perception of Egomotion," *Journal of Experimental Psychology: Human Perception and Performance*, Vol. 2, No. 3, 1976, pp. 448–456.

[7]Warren, R., "Optical Transformation During Movement," Air Force Office of Scientific Research, Rept. AFOSR-TR-82-1028, NTIS AD-A122 275/1, Ohio State Univ., Columbus, OH, Oct. 1982.

[8]Zacharias, G. L., "Flow-Field Cueing Conditions for Inferring Observer Self-Motion," Bolt Beranek and Newman, Inc., Rept. 5118, Cambridge, MA, Sept. 1982.

[9]Zacharias, G. L., Caglayan, A. K., and Sinacori, J. B., "A Visual Cueing Model for Terrain-Following Applications," *Journal of Guidance, Control, and Dynamics*, Vol. 8, No. 2, 1985, pp. 201–207.

[10]Denton, G. G., "The Influence of Visual Pattern on Perceived Speed," *Perception*, Vol. 9, 1980, pp. 393–402.

[11]Owen, D. H., Wolpert, L., and Warren, R., "Effects of Optical Flow Acceleration, Edge Acceleration, and Viewing Time on the Perception of Egospeed Acceleration," NASA Scientific and Technical Information Facility, 1984, pp. 79–140.

[12]Johnson, W. W., Bennett, C. T., O' Donnell, K., and Phatak, A. V., "Optical Variables Useful in the Active Control of Altitude," *Proceedings of the 23rd Annual Conference on Manual Control* (Cambridge, MA), June 1988.

[13]Awe, C. A., Johnson, W. W., and Schmitz, F., "Inflexibility in Selecting the Optical Basis for Perceiving Speed," *Proceedings of the Human Factors Society 33rd Annual Meeting*, 1989, pp. 1440–1444.

[14]Larish, J. F., and Flach, J. M., "Sources of Optical Information Useful for the Perception of Velocity of Rectilinear Selfmotion," *Journal of Experimental Psychology: Human Perception and Performance*, Vol. 16, No. 2, 1990, pp. 295–302.

[15]Naish, J. M., "Control Information in Visual Flight," Seventh Annual Conf. on Manual Control, Univ. of Southern California, Los Angeles, CA, June 1971.

[16]Wewerinke, P. H., "A Theoretical and Experimental Analysis of the Outside World Perception Process," Fourteenth Annual Conf. on Manual Control, Univ. of Southern California, Los Angeles, CA, April 1978.

[17]Wewerinke, P. H., "The Effect of Visual Information on the Manual Approach and Landing," Sixteenth Annual Conf. on Manual Control, Massachusetts Inst. of Technology, Cambridge, MA, May 1980, pp. 49–65.

[18]Grunwald, A. J., and Merhav, S. J., "Vehicular Control by Visual Field Cues—Analytical Model and Experimental Validation," *IEEE Transactions on Systems, Man and Cybernetics*, Vol. 6, No. 12, 1976, pp. 835–845.

[19]Merhav, S. J., and Grunwald, A. J., "Display Augmentation in Manual Control of Remotely Piloted Vehicles," *Journal of Aircraft*, Vol. 15, No. 3, 1978, pp. 182–189.

[20]Grunwald, A. J., and Merhav, S. J., "Effectiveness of Basic Display Augmentation in Vehicular Control by Visual Field Cues," *IEEE Transactions on Systems, Man and Cybernetics*, Vol. 8, No. 9, 1978, pp. 679–690.

[21]Schmidt, D. K., and Silk, A. B., "Modeling Human Perception and Estimation of Kinematic Responses During Aircraft Landing," *Proceedings of the Guidance, Navigation, and Control Conference* (Minneapolis, MN), AIAA, Washington, DC, 1988, pp. 1117–1126.